Acta Crystallographica Section B
Structural Science
ISSN 0108-7681

Reversible phase transitions in Na_2S under pressure: a comparison with the cation array in Na_2SO_4

A. Vegas,[a]*† A. Grzechnik,[a] K. Syassen,[a] I. Loa,[a] M. Hanfland[b] and M. Jansen[a]

[a]Max-Planck Institut für Festkörperforschung, Heisenbergstrasse 1, D-70569 Stuttgart, Germany, and [b]European Synchrotron Radiation Facility, BP 220, F-38000 Grenoble, France

† Also at: Instituto de Química-Física Rocasolano, CSIC, Serrano 119, E-28006 Madrid, Spain.

Correspondence e-mail: avegas@iqfr.csic.es

Received 7 July 2000
Accepted 7 November 2000

The structural behavior of the antifluorite Na_2S, disodium sulfide, has been studied under pressure up to 22 GPa by *in situ* synchrotron X-ray diffraction experiments in a diamond anvil cell at room temperature. At approximately 7 GPa, Na_2S undergoes a first phase transition to the orthorhombic anticotunnite ($PbCl_2$) structure (*Pnma*, $Z = 4$). The lattice parameters at 8.2 GPa are $a = 6.707\ (5)$, $b = 4.120\ (3)$, $c = 8.025\ (4)$ Å. At approximately 16 GPa, Na_2S undergoes a second transition adopting the structure of the Ni_2In-type ($P6_3/mmc$, $Z = 2$). The lattice parameters at 16.6 GPa are $a = 4.376\ (18)$, $c = 5.856\ (9)$ Å. Both pressure-induced phases have been confirmed by full Rietveld refinements. An inspection of the cation array of Na_2SO_4 reveals that its Na_2S subarray is also of the Ni_2In-type. This feature represents a new example of how the cation arrangements in ternary oxides correspond to the topology of the respective binary compounds. We discuss analogies between the insertion of oxygen and the application of pressure.

1. Introduction

In 1985, O'Keeffe and Hyde reported a new approach to describe the crystal structures of oxides (O'Keeffe & Hyde, 1985). In their model, emphasis was given to the cation subarrays which, in many instances, adopt the structure of either elements or simple alloys, the oxides being regarded as oxygen-stuffed alloys. Among the examples given, some present the peculiarity that both the cation array and the corresponding alloy have the same structure and almost identical unit-cell dimensions, as if the O/F atoms were inserted into the interstitial sites of the element/alloy without any significant volume increase. This is the case of the phases Ca_2Si–Ca_2SiO_4 and Ca–CaF_2 (O'Keeffe & Hyde, 1985).

It has been pointed out that these striking examples are not isolated cases. For instance, the pairs of compounds CaGe–$CaGeO_3$ (Martínez-Cruz *et al.*, 1994), Al*Ln*–Al*Ln*O_3 (Ramos-Gallardo & Vegas, 1997), Cs_3Bi–Cs_3BiO_3 (Zoche & Jansen, 1997) and Yb–YbOOH (Vegas & Isea, 1997) also exhibit similar behavior. The same has been observed for the high-pressure modification of the BaSn alloy (CsCl-type) and the cubic perovskite $BaSnO_3$, both having the same topology and dimensions (Martínez-Cruz *et al.*, 1994). In the latter case a correlation has been established between oxidation and pressure in the sense that the oxide adopts a cation arrangement of a high-pressure phase of the alloy (Martínez-Cruz *et al.*, 1994). Moreover, it has been suggested (Vegas & Martínez-Cruz, 1995; Vegas, 2000) that, in many oxides, the cation arrays could be regarded as metastable analogues of element/alloy phases which might exist under extreme conditions of pressure

and/or temperature and which are stabilized by the presence of the O atoms in the oxides.

These ideas led us to study simple binary compounds at high pressures to see whether new phases occur and whether they are topologically related to the cation subarrays in the corresponding oxides. Such an approach had previously been suggested by Martínez-Cruz *et al.* (1994).

It is known that the fluorite-type compounds undergo phase transitions under pressure, following the sequence fluorite → cotunnite → Ni_2In (Leger *et al.*, 1995; Leger & Haines, 1997). It can be expected that the antifluorite-type compounds would follow a similar path. In a previous paper we have reported on the antifluorite → anticotunnite transition in Li_2S (Grzechnik *et al.*, 2000). Here we present a high-pressure study of antifluorite Na_2S (Zintl *et al.*, 1934), whose high-pressure phases will be compared with the cation arrays in the structures of Na_2SO_4. The high-pressure experiments were carried out by *in situ* synchrotron angle-dispersive X-ray diffraction using a diamond anvil cell (DAC) at room temperature.

2. Experimental

Finely ground samples of Na_2S (Alfa-Aesar) with 99.9% nominal purity were used for all experiments. A preliminary X-ray diffraction experiment with Cu $K\alpha$ radiation revealed the absence of any impurity in the sample. A least-squares refinement of the 2θ values for 14 reflections, with silicon as the internal standard, led to the unit-cell parameter a = 6.5384 (1) Å, V = 279.52 Å^3 in an acceptable agreement with the previously reported value (a = 6.526 Å) by Zintl *et al.* (1934).

The high-pressure XRD experiments up to 22 GPa (T = 298 K) were carried out on the same batch of the sample. The Na_2S fine powder was always handled in glove boxes. It was loaded into the diamond anvil cells without any pressure medium.

Angle-dispersive X-ray powder diffractograms were measured on the ID9 beamline at the European Synchrotron Radiation Facility (Grenoble). Monochromatic radiation at λ = 0.43171 Å was used for pattern collection on image plates. The images were integrated using the program *FIT2D* (Hammersley *et al.*, 1996) to yield intensity *versus* 2θ diagrams. The instrumental resolution (a minimum full-width at half height of diffraction peaks) was 0.03°. To improve powder averaging, the DAC was rotated by ± 3°. The ruby luminescence method (Mao *et al.*, 1986) was used for pressure calibration.

The sensitivity of Na_2S precluded any use of a pressure medium since there is no fully hydrostatic medium that could be loaded together with such a sample into a diamond anvil cell. It should be pointed out that, unlike in covalent solids, the non-hydrostatic effects in ionic compounds are not severe. In the case of our sample, this was confirmed by well resolved ruby luminescence bands in the entire pressure range studied here. On the other hand, pressure inhomogeneity could also affect the quality of the powder patterns and, hence, their full Rietveld refinements. For this reason, the Stephens function (Stephens, 1999) was used in this work, as it incorporates the anisotropic broadening of reflections due to strain, stacking faults, shear stress and other effects that could develop under not purely hydrostatic conditions.

Table 1
Final atomic parameters for the anticotunnite structure of Na_2S at 8.2 GPa.

	x	y	z
S	0.2457(5)	1/4	−0.1157(2)
Na(1)	0.0173(7)	1/4	0.1851(3)
Na(2)	0.1517(6)	1/4	0.5758(4)

3. Results

Diffraction diagrams measured at different pressures are shown in Fig. 1. At pressures up to approximately 4.4 GPa all the diffraction lines correspond to the cubic antifluorite structure. At 6.4 GPa additional peaks appear, indicating the onset of a phase transition. At 7.6 GPa the reflections corresponding to the antifluorite phase completely disappear. However, the peaks of the new phase were broad and weak, indicating the poor crystallinity of the sample. After annealing, at 423 K for 3 h, the diffractogram taken at a pressure of 8.2 GPa showed sharper and more intense reflections. All the X-ray peaks of the new phase at 8.2 GPa were

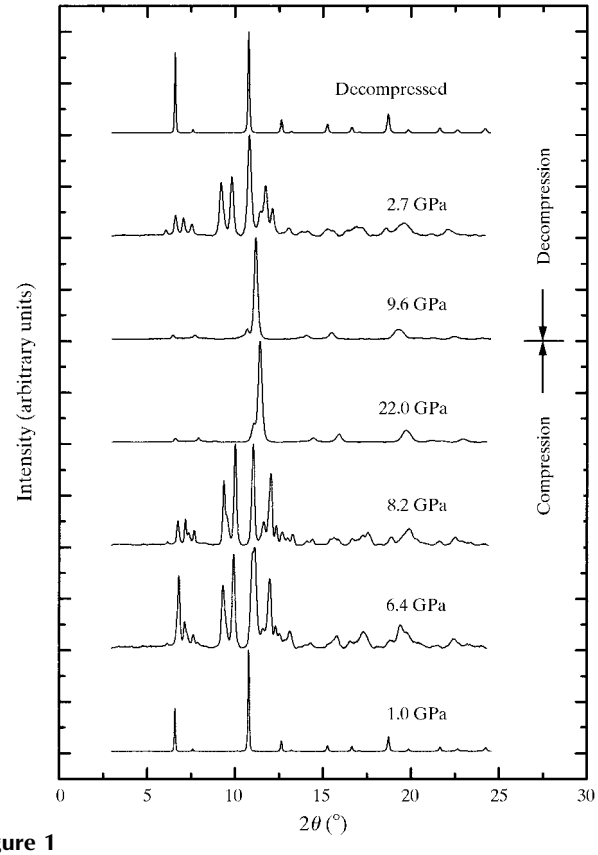

Figure 1
Normalized X-ray powder diffraction patterns of Na_2S at different pressures. The wavelength is λ = 0.43171 Å. Backgrounds are subtracted.

Table 2
Interatomic distances (in Å) in the anticotunnite phase of Na_2S at 8.2 GPa.

Na–Na Prisms		Na–Na Interprisms		S–Na	
Na(1)—Na(2)^{i}	3.220 (5)	Na(2)^{iv}—Na(1)^{i}	3.034 (3)	S—Na(2)^{vii}	2.557 (4)
Na(1)^{ii}—Na(2)^{iii}	3.220 (5)	Na(2)^{iv}—Na(1)^{iii}	3.034 (3)	S—Na(2)^{viii}	2.660 (3)
Na(1)^{i}—Na(2)^{i}	3.264 (4)	Na(2)^{iv}—Na(2)^{i}	3.136 (5)	S—Na(2)^{ix}	2.660 (3)
Na(1)^{iii}—Na(2)^{iii}	3.264 (4)	Na(2)^{iv}—Na(2)^{iii}	3.136 (5)	S—Na(2)^{x}	2.742 (5)
Na(1)—Na(1)^{i}	3.510 (1)	Na(2)^{iv}—Na(1)^{v}	3.148 (5)	S—Na(1)^{xi}	2.765 (4)
Na(1)^{ii}—Na(1)^{iii}	3.510 (1)	Na(2)^{iv}—Na(1)^{v}	3.148 (5)	S—Na(1)^{xii}	2.765 (4)
Na(1)—Na(1)^{ii}	4.119 (1)	Na(1)^{vi}—Na(1)^{i}	3.625 (4)	S—Na(2)^{vii}	2.558 (4)
Na(1)^{i}—Na(1)^{iii}	4.119 (1)	Na(1)^{vi}—Na(1)^{iii}	3.625 (4)	S—Na(1)^{viii}	3.051 (4)
Na(2)^{i}—Na(2)^{iii}	4.119 (1)			S—Na(1)^{ix}	3.051 (4)

Symmetry codes: (i) $x-\frac{1}{2}, y, \frac{1}{2}-z$; (ii) $x, 1+y, z$; (iii) $x-\frac{1}{2}, 1+y, \frac{1}{2}-z$; (iv) $-\frac{1}{2}-x, 1-y, z-\frac{1}{2}$; (v) $x-1, y, z$; (vi) $-\frac{1}{2}-x, 1-y, \frac{1}{2}+z$; (vii) $x, y, z-1$; (viii) $\frac{1}{2}-x, 1-y, z-\frac{1}{2}$; (ix) $\frac{1}{2}-x, -y, z$; (x) $\frac{1}{2}+x, y, \frac{1}{2}-z$.

indexed by means of the program *DICVOL* (Boultif & Louer, 1991) on the basis of an orthorhombic cell of dimensions a = 6.707 (5), b = 4.120 (3), c = 8.025 (4) Å (M_{20} = 7.1, F_{20} = 27.9). The volume V = 221.74 Å^3 indicated that the number of Na_2S formula units in the unit cell is Z = 4. The systematic extinctions, consistent with the space group *Pnma*, together with the unit-cell dimensions suggested that the new orthorhombic phase could have the anticotunnite (*anti*-$PbCl_2$) structure. A full Rietveld profile refinement of the pattern at 8.2 GPa (Fig. 2) was carried out using the program *GSAS* (Larson & Von Dreele, 1994). The starting atomic coordinates were those of the Cs and S atoms in Cs_2S (Sommer & Hoppe, 1977). There were no constraints on minimal Na—S and Na—Na distances. The refined parameters were: the fractional coordinates, isotropic thermal parameters, Chebyshev polynomial background (four terms), Stephens profile function (Stephens, 1999), cell parameters and the March–Dollase correction for preferred orientation. The same strategy and sets of structural and global parameters were used for the other Rietveld refinements discussed below. The refinement converged to $R(F^2)$ = 0.08. The final atomic and lattice parameters are given in Table 1 and the interatomic distances are collected in Table 2. A projection of the structure is represented in Fig. 3.

The anticotunnite phase is stable up to 12.3 GPa. At 16.6 GPa a completely new diffraction pattern is observed. This indicates the existence of a second phase transition to a structure which is stable up to at least 22.0 GPa. This third polymorph can be decompressed down to at least 9.6 GPa. To index the corresponding diffractogram, only the sharp and well resolved peaks were taken into account. The reflections could be indexed (Boultif & Louer, 1991) on the basis of a hexagonal cell of dimensions a = 4.4269 (2), c = 5.815 (2) Å at 9.6 GPa (M_{11} = 24.5, F_{11} = 33.9). The volume V = 99.03 Å^3 points towards Z = 2. The systematic extinctions, consistent with the space group $P6_3/mmc$, together with the cell dimensions, lead to a structure assignment of the Ni_2In type. This structure has all the atoms in special positions with all the coordinates fixed: S at 2(*c*) (1/3, 2/3, 1/4;); Na(1) at 2(*a*) (0, 0, 0) and Na(2) at 2(*d*) (1/3, 2/3, 3/4). To confirm this structure a Rietveld refinement was carried out, following the stategy described above, with the data collected in the decompression run at 9.6 GPa. Convergence was achieved at $R(F^2)$ = 0.126. The interatomic distances are collected in Table 3. The observed and calculated diffractogram is represented in Fig. 2 and the structure is drawn in Fig. 4.

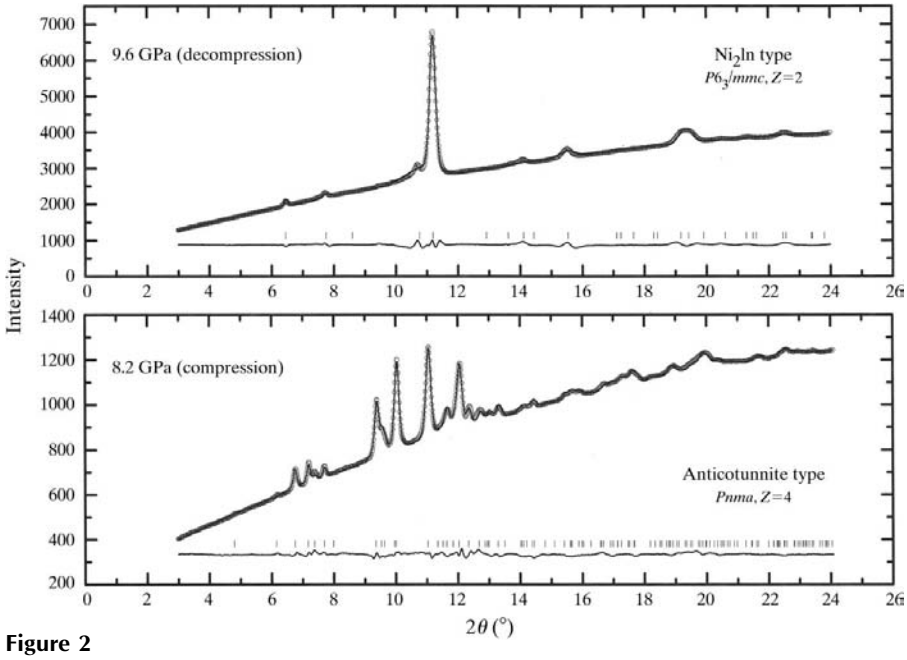

Figure 2
Observed, calculated and difference X-ray diffraction profiles of both orthorhombic Na_2S and hexagonal Na_2S. Vertical markers indicate Bragg reflections.

The pressure dependence of the volume per Na_2S formula unit, in all the three phases, is shown in Fig. 5. Both phase transitions, antifluorite → anticotunnite and anticotunnite → Ni_2In, are first order in character with relative volume changes of 8% at 6.4 GPa and 10% at 16.6 GPa, respectively.

It should be noted that all the observed transformations are reversible and antifluorite structured Na_2S is recovered at ambient pressure. Upon decompression, large hysteresis is observed and the Ni_2In and anticotunnite types are stable down to at least 9.6 and 2.7 GPa, respectively.

4. Discussion

The results of this study show that, at room temperature, Na_2S undergoes two reversible phase transitions, *i.e.* an anti-

Table 3
Interatomic distances (in Å) in the Ni_2In phase of Na_2S at 9.2 GPa (e.s.d.'s 0.003 Å).

Na—Na Prisms		Na—Na Interprisms		S—Na	
$Na(1)^{i}$—$Na(1)^{ii}$	2.914	$Na(2)$—$Na(1)^{xi}$	2.943	S—$Na(2)^{xv}$	2.557
$Na(1)^{iii}$—$Na(1)^{iv}$	2.914	$Na(2)$—$Na(1)^{xii}$	2.943	S—$Na(2)^{xvi}$	2.557
$Na(1)^{i}$—$Na(2)^{v}$	2.943	$Na(2)$—$Na(1)^{xii}$	2.943	S—$Na(2)^{xvii}$	2.557
$Na(1)^{iii}$—$Na(2)^{vi}$	2.943	$Na(2)$—$Na(1)^{xiii}$	2.943	S—$Na(2)$	2.914
$Na(1)^{ii}$—$Na(2)^{vii}$	2.943			S—$Na(2)^{xviii}$	2.914
$Na(1)^{iv}$—$Na(2)^{viii}$	2.943			S—$Na(1)$	2.943
$Na(1)^{ix}$—$Na(1)^{x}$	4.429			S—$Na(1)^{ix}$	2.943
$Na(1)^{ii}$—$Na(1)^{iv}$	4.429			S—$Na(1)^{x}$	2.943
$Na(2)^{ii}$—$Na(2)^{iv}$	4.429			S—$Na(1)^{xi}$	2.943
				S—$Na(1)^{xii}$	2.943
				S—$Na(1)^{ii}$	2.943

Symmetry codes: (i) $x, y, 1+z$; (ii) $x-y, x, \frac{1}{2}+z$; (iii) $1+x, y, 1+z$; (iv) $1+x-y, x, \frac{1}{2}+z$; (v) $x-y, x-1, \frac{1}{2}+z$; (vi) $1+x-y, x-1, \frac{1}{2}+z$; (vii) $x-y, x-1, z-\frac{1}{2}$; (viii) $1+x-y, x-1, z-\frac{1}{2}$; (ix) $x, 1+y, z$; (x) $1+x, 1+y, z$; (xi) $x-y, 1+x, \frac{1}{2}+z$; (xii) $1+x-y, 1+x, \frac{1}{2}+z$; (xiii) $x, 1+y, 1+z$; (xiv) $1+x, 1+y, 1+z$; (xv) $x-y, x, z-\frac{1}{2}$; (xvi) $1+x-y, x, z-\frac{1}{2}$; (xvii) $1+x-y, 1+x, z-\frac{1}{2}$; (xviii) $x, y, z-1$.

fluorite → anticotunnite transition at approximately 7 GPa and a further anticotunnite → Ni_2In transition at approximately 16 GPa. For Na_2S these transitions could be expected because Li_2S also undergoes a pressure-induced antifluorite → anticotunnite transition at approximately 12 GPa (Grzechnik *et al.*, 2000), while Cs_2S adopts the anticotunnite structure at ambient pressure (Sommer & Hoppe, 1977). The behavior of Na_2S resembles that of BaF_2, which also follows the transition path fluorite → cotunnite → Ni_2In at high pressures (Leger *et al.*, 1995), corresponding to the following coordination changes of the cation: 8 → 9 → 11, respectively.

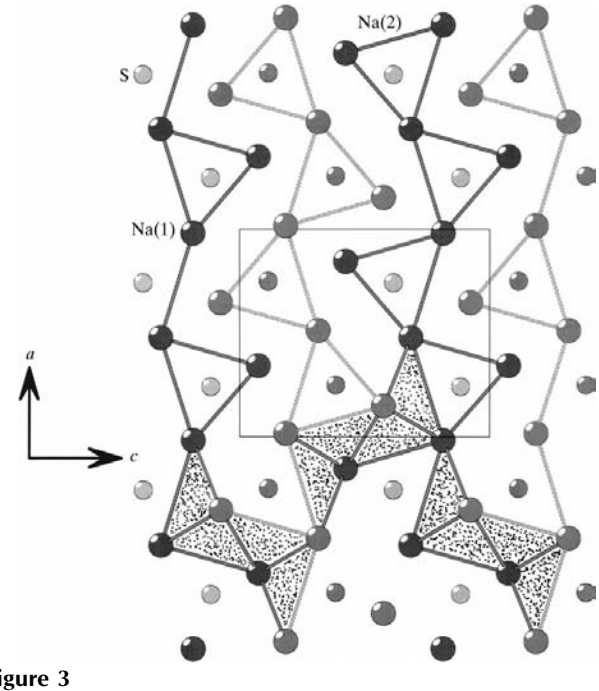

Figure 3
Crystal structure of anticotunnite Na_2S at 8.2 GPa, projected along the *b* axis, showing the zigzag chains of trigonal prisms. At the bottom, the clusters defined by Simon (1981) are shaded. Large and small circles are Na and S atoms, respectively. Black and grey circles represent atoms at $y = \frac{1}{4}$ and $y = \frac{3}{4}$, respectively.

4.1. Description of the structures

The anticotunnite structure can be described following the model of Sommer & Hoppe (1977) for Cs_2S, *i.e.* the S atoms form an irregular *h.c.p.* array in which all the octahedral holes are occupied by Na(2), whereas Na(1) atoms are inserted into one half of the tetrahedral holes. The Na(2) atoms are slightly shifted off the center of the octahedron leading to a coordination number of 5 + 1. Looking at the distances given in Table 2, it is seen that seven of the nine S—Na distances are shorter than those of the antifluorite phase (2.819 Å) at ambient pressure. The anticotunnite structure can also be described in terms of chains of triangular prisms of Na atoms (see Fig. 3). The prisms are sharing lateral edges and form walls parallel to the *ab* plane. All atoms in the structure are situated at $y = \frac{1}{4}, \frac{3}{4}$, so that adjacent walls are shifted by *b*/2. The S atoms are lodged into these trigonal prisms and are coordinated by nine Na atoms, six of them forming the prisms and three additional Na atoms which cap the lateral faces of the prisms, which belong to adjacent walls and are situated at the same *y* coordinate as the S atoms. The two crystallographically independent Na atoms have different coordination numbers. Na(1) atoms are fourfold coordinated into an S_4 tetrahedron and the Na(2) atoms are hexacoordinated into an S_6 octahedron. A third way of describing this structure is by means of the clusters depicted at the bottom of Fig. 3 (Simon, 1981; Vegas & Martínez-Ripoll, 1992). These clusters are fragments of either a b.c.c. (body-centered cubic) or f.c.c. (face-centered cubic) net.

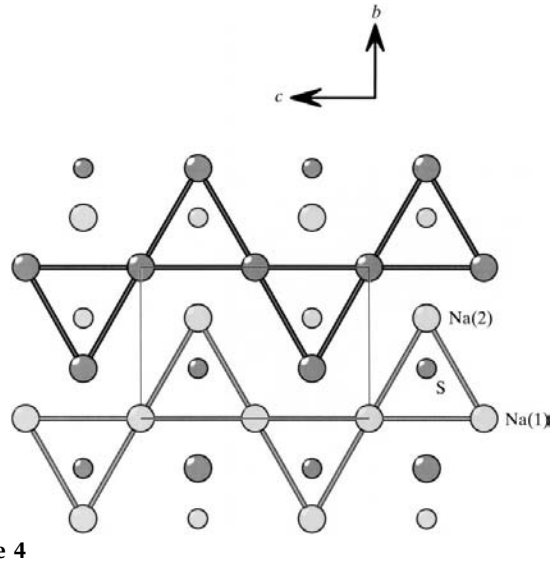

Figure 4
The crystal structure of the Ni_2In-type phase of Na_2S viewed along the *a* axis. Large and small circles represent Na and S atoms, respectively. Dark and light circles are shifted by *a*/2 with respect to each other.

Table 4
Na—Na and S—Na distances (in Å) in the Ni_2In-type array of the Na_2SO_4 (I, II and III) phases.

Phase	Na—Na prisms	Na—Na interprisms	S—Na
Na_2SO_4-I	2 × 3.67	4 × 3.64	3 × 3.14
	4 × 3.64		6 × 3.64
	3 × 5.44		2 × 3.67
Na_2SO_4-II	2 × 3.57	2 × 3.42	1 × 3.10
	4 × 3.74	2 × 3.61	1 × 3.15
	3 × 5.31		1 × 3.09
			2 × 3.54
			2 × 3.66
			2 × 3.57
			2 × 3.58
Na_2SO_4-III	2 × 3.49	4 × 3.72	1 × 3.05
	4 × 3.29		2 × 3.16
	3.293 × 5.63		4 × 3.57
			2 × 3.50
			2 × 3.58

Comparing Figs. 3 and 4, it can be seen that the Ni_2In-type structure is closely related to that of anticotunnite. The walls of trigonal prisms are present in both structures, but whereas they are puckered (zigzag) in the $PbCl_2$-type structure, they are stretched in the Ni_2In-type phase. The result of this transformation is an increase in the coordination number of the S atoms from 9 (anticotunnite) to 11 (Ni_2In). A diffusionless mechanism was proposed (O'Keeffe & Hyde, 1985) for a similar transition existing in K_2SO_4 at high temperature. Three of the 11 Na—S distances for the new phase (see Table 3) are much shorter (2.54 Å) than those of the anticotunnite structure at 8.2 GPa.

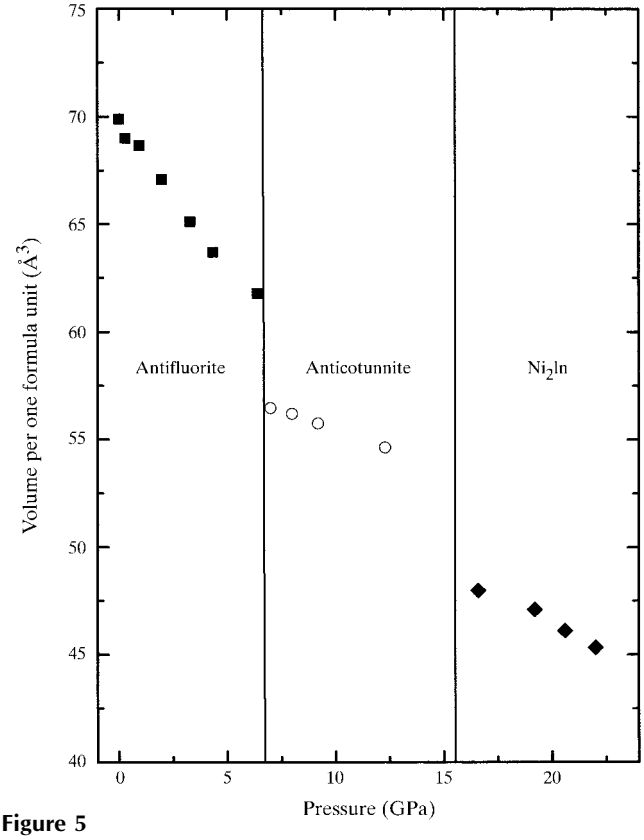

Figure 5
Pressure dependence of volumes per formula unit, under compression, for the three phases of Na_2S. $Z = 4$ for the cubic (antifluorite) and the orthorhombic (anticotunnite) phases and $Z = 2$ for the hexagonal (Ni_2In-type) phase.

4.2. Na_2S and Na_2SO_4

An interesting aspect of this work is to compare the structures of Na_2S with the cation array of the Na_2SO_4 oxide. At ambient pressure, four phases are known for sodium sulfate (Rasmussen *et al.*, 1996). At room temperature, the stable phase is Na_2SO_4-V (thenardite, *Fddd*). Its cation array forms a network which is related to the cation array of spinels. At higher temperatures the phases −III (463 K, *Cmcm*, $Z = 4$), −II (493 K, *Pbnm*, $Z = 4$) and −I (543 K, $P6_3/mmc$, $Z = 2$) have been observed. These three phases are isotypic with olivine (Mg_2SiO_4) and one of them (the phase II) is isostructural with it. As occurs with all the olivine-like structures (O'Keeffe & Hyde, 1985), the Na_2S subarrays, in the high-temperature phases I, II and III of Na_2SO_4, are of the Ni_2In-type (see Fig. 6). Moreover, the space group of phase I ($P6_3/mmc$) is the same as that of the high-pressure phase of Na_2S itself. Thus, the structure of the high-pressure phase of the Na_2S binary compound has been stabilized in the ternary oxide Na_2SO_4. Also, in this case we can establish a correlation between oxidation and pressure as it has been observed in the system BaSn–$BaSnO_3$ (Martínez-Cruz *et al.*, 1994). However, in this case we can quantify the pressure effect of the O atoms. Insertion of four O atoms per Na_2S virtually produces the same effect as the pressure of 16 GPa, stabilizing the Ni_2In-type structure of Na_2S. However, the similarity between the Na_2S arrangements only applies to the topology. With respect

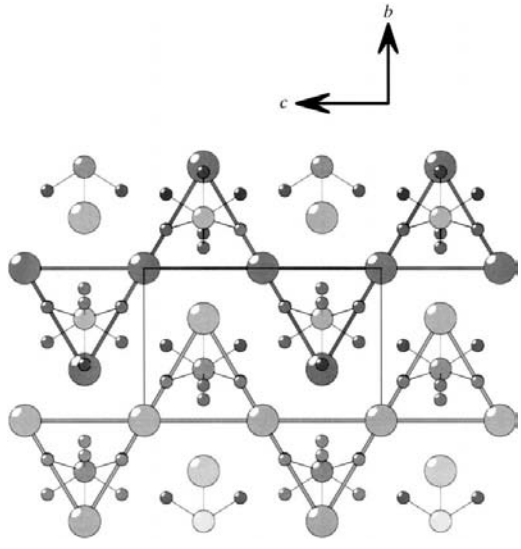

Figure 6
The crystal structure of the high-temperature phase Na_2SO_4-I ($P6_3/mmc$, 543 K) projected along the *b* axis. The Na_2S subarray (Ni_2In type) has been outlined by drawing the Na–Na contacts forming the trigonal prisms where the S atoms are inserted (compare with Fig. 4). Adjacent chains of trigonal prisms are shifted by half of the projection axis. Large, medium and small circles represent Na, S and O atoms, respectively. The figure shows the disorder observed in the O atoms.

to dimensions, the structure of Na_2SO_4-I is an expansion of the topologically equivalent Ni_2In-type structure of Na_2S. This expansion precludes any interpretation of the similarity in topologies in terms of the similar size of the S^{2-} and SO_4^{2-} anions. Table 4 summarizes all the Na—Na and the 11 S—Na distances for the three high-temperature phases of Na_2SO_4 for a comparison with the corresponding data for Na_2S, which were collected in Table 3.

A comparison of the structures of sulfides and sulfates reveals that this is not the only example in which the structure of the sulfide is reproduced in the sulfate. Thus, the antifluorite structure of Li_2S is found in the high-temperature phase of Li_2SO_4 (Nilsson *et al.*, 1980) and the anticotunnite structure of Cs_2S is reproduced in the room-temperature phase of Cs_2SO_4 (Weber *et al.*, 1989).

The anticotunnite-type structure is not observed in any of the four modifications of Na_2SO_4. It is known that at relatively low pressures (up to 3 GPa) and temperatures from 373 to 573 K, two additional phases seem to exist, as deduced from DTA studies (Pistorius, 1965; Secco & Secco, 1992) with a possibility that any of these phases could form the anticotunnite structure for the Na_2S subarray. X-ray high-pressure experiments would be interesting in order to determine the structure of these HP polymorphs.

5. Conclusions

This high-pressure study provides a new example of how, in oxides, the cation arrays maintain the structure of the corresponding binary compound under pressure, allowing for a correlation between oxidation and pressure. The similarity of the cation sublattices of the high-temperature phase of Li_2SO_4, Na_2SO_4 and Cs_2SO_4 to Li_2S (antifluorite), Na_2S (Ni_2In) and Cs_2S (anticotunnite), respectively, seems to support the idea that, although no chemical bond is to be expected between the cations, some kind of recognition could exist between them, in spite of being embedded in an oxygen matrix. The recognition does not only produce similar topologies of the Na_2S arrays, but also comparable values of the Na—Na distances in both the sulfate and the Na metal. From the work reported here, it is clear that the analysis of the cation arrays is not a mere descriptive tool. We believe that such structural relationships between alloys and oxides could be helpful for understanding the systematics of pressure-induced phase transitions in these materials.

References

Boultif, A. & Louer, D. (1991). *J. Appl. Cryst.* **24**, 987–993.
Grzechnik, A., Vegas, A., Syassen, K., Loa, I., Hanfland, M. & Jansen, M. (2000). *J. Solid State Chem.* **154**, 603–611.
Hammersley, A. P., Svensson, S. O., Hanfland, M., Fitch, A. N. & Häusermann, D. (1996). *High Press. Res.* **14**, 235–248.
Larson, A. C. & Von Dreele, R. B. (1994). *GSAS*, Report No. LAUR 86-784. Los Alamos National Laboratory, Los Alamos, New Mexico, USA.
Leger, J. M. & Haines, J. (1997). *Eur. J. Solid State Inorg. Chem.* **34**, 785–796.
Leger, J. M., Haines, J., Atouf, A., Schulte, O. & Hull, S. (1995). *Phys. Rev. B*, **52**, 13247–13256.
Mao, H. K., Xu, J. & Bell, P. M. (1986). *J. Geophys. Res.* **91**, 4673–4676.
Martínez-Cruz, L. A., Ramos-Gallardo, A. & Vegas, A. (1994). *J. Solid State Chem.* **110**, 397–398.
Nilsson, L., Thomas, J. O. & Tofield, B. C. (1980). *J. Phys. C*, **13**, 6441–6451.
O'Keeffe, M. & Hyde, B. G. (1985). *Structure and Bonding*, Vol. 61, pp. 77–144. Berlin: Springer Verlag.
Pistorius, C. W. F. T. (1965). *J. Chem. Phys.* **43**, 2895–2898.
Ramos-Gallardo, A. & Vegas, A. (1997). *J. Solid State Chem.* **128**, 69–72.
Rasmussen, S. E., Jorgensen, J. E. & Lundtoft, B. (1996). *J. Appl. Cryst.* **29**, 42–47.
Secco, R. A. & Secco, E. A. (1992). *J. Phys. Chem. Solids*, **53**, 749–753.
Simon, A. (1981). *Angew. Chem. Int. Ed. Engl.* **20**, 1–22.
Sommer, H. & Hoppe, R. (1977). *Z. Anorg. Allg. Chem.* **429**, 118–130.
Stephens, P. W. (1999). *J. Appl. Cryst.* **32**, 281–289.
Vegas, A. (2000). *Crystallogr. Rev.* **7**, 189–286.
Vegas, A. & Isea, R. (1997). *J. Solid State Chem.* **131**, 358–362.
Vegas, A. & Martínez-Cruz, L. A. (1995). *Z. Kristallogr.* **210**, 581–584.
Vegas, A. & Martínez-Ripoll, M. (1992). *Acta Cryst.* B**48**, 747–752.
Weber, H. J., Schulz, M., Schmitz, S., Granzin, J. & Siegert, H. (1989). *J. Phys. Condensed Matter*, **1**, 8543–8557.
Zintl, E., Harder, A. & Dauth, B. (1934). *Z. Elektrochem.* **40**, 588–593.
Zoche, N. & Jansen, M. (1997). *Z. Anorg Allg. Chem.* **623**, 832–836.